Vibrational Energy Transfer in Highly Excited Bridged Azulene-Aryl Compounds: Direct Observation of Energy Flow through Aliphatic Chains and into the Solvent†

D. Schwarzer,* C. Hanisch, P. Kutne, and J. Troe

Max-Planck-Institut für Biophysikalische Chemie, Am Fassberg, 37077 Göttingen, Germany

Received: April 25, 2002; In Final Form: June 19, 2002

Intra- and intermolecular vibrational energy flow in vibrationally highly excited bridged azulene-$(CH_2)_n$-aryl (n = 0,1,3; aryl = benzene or anthracene) compounds is observed using time-resolved pump−probe laser spectroscopy. Light absorption in the azulene S_1-band, followed by fast internal conversion, leads to vibrational excitation at the azulene side of the molecules. Subsequent energy flow through the aliphatic chain to the aryl group at the other side of the molecules and vibrational energy transfer into a surrounding liquid solvent bath are measured either by probing the red edge of the azulene S_3-absorption band at 300 nm and/or the anthracene S_1-absorption band at 400 nm. The data are analyzed by representing the intramolecular energy flux as a diffusion process and using hot absorption spectra of the two chromophores of the compounds for measuring their energy contents. A fit to all of the experimental signals leads to an energy conductivity of a single C−C bond of $\kappa_{CC} = (10 \pm 1)$ cm^{-1} K^{-1} ps^{-1} (with energies measured in cm^{-1}). Depending on the substituent and the length of the chain, this models yield intramolecular energy transfer times of 1.2−4 ps. Energy transfer to the solvent 1,1,2-trichloro-trifluoro-ethane, on the other hand, is characterized by an exponential loss profile with a cooling time constant of (21 ± 2) ps, independent of the substituent and the same as for bare azulene.

I. Introduction

Intra- and intermolecular vibrational energy flow are essential dynamical processes which determine rates, pathways, and efficiencies of chemical reactions. Once a polyatomic molecule has been excited by some activation process, intramolecular vibrational energy redistribution (IVR) is the primary elementary process which exchanges the energy among the vibrational degrees of freedom inside the molecule.[1] The assumption of rapid IVR is of central importance for statistical unimolecular rate theories.[2,3] In the presence of a bath gas or in solution, vibrational energy of the reactant can also be exchanged with the surrounding by collision-induced intermolecular vibrational energy transfer (CET). At the same time, IVR rates can be enhanced by anharmonic couplings introduced into the reactant during the collision, a process termed "solvent assisted IVR". Under gas phase conditions, for large polyatomic molecules at high excitation energy, a separation of time scales between IVR and CET is usually assumed, i.e., between two collisions a statistical distribution of the energy inside the molecule is generally established. This is certainly true when the time between collisions is sufficiently long. In liquid solution, however, CET can be very fast and since the energy transfer process is mode selective, namely most efficient for low-frequency vibrational modes, it might happen that IVR is incomplete with respect to these modes before the next energy-transferring collision occurs.

Collisional energy transfer experiments on highly excited azulene in supercritical fluids[4,5] have shown that the density dependence of the CET rate can be well understood in the framework of the isolated binary collision (IBC) model.[6] This approach suggests that vibrational energy transfer proceeds only via binary interactions and that the relaxation probability per collision is just the same for both gas and liquid phase. Corresponding computer simulations, however, clearly demonstrate a reduction of the energy transfer efficiency of low-frequency vibrational modes at liquid densities[7,8] indicating a change of the energy transfer mechanism and, therefore, a breakdown of the IBC approach. Recent molecular dynamics studies on the IVR/CET dynamics of CH_2I_2 in $CDCl_3$ have shown that in small molecules with slower IVR rates (due to a lower density of states) the energy transfer efficiency of low-frequency vibrational modes in solution can be reduced to an extent that they merely act as spectators during the CET process.[9]

Most information on IVR in the ground electronic state stems from frequency resolved experiments on isolated molecules in the gas phase or in supersonic jets (e.g., reviews in refs 1, 10, and 11). By resolving features and analyzing widths, splittings and relative intensities of lines within spectral clumps (the zeroth-order bright states), details about IVR mechanisms were obtained. From these studies it is known that IVR very often is a hierarchical process proceeding via sequential couplings between tiers of states. Unfortunately, such frequency domain experiments are sensitive mainly to the primary steps in the IVR cascade, i.e., extracted IVR lifetimes are dominated by the first tier in the hierarchical sequence of relaxation paths. Little or no information can be gained from the spectra how fast vibrational energy finally flows into modes associated with higher tiers. This problem can be solved by means of two-color pump−probe techniques when the probe light independently interrogates chromophores (and thereby eigenstates) of the molecule which do not directly couple to the initially excited

† This paper is dedicated to the memory of Dr. Bernhard Nickel.

10.1021/jp0210576 CCC: $22.00
Published on Web 08/09/2002

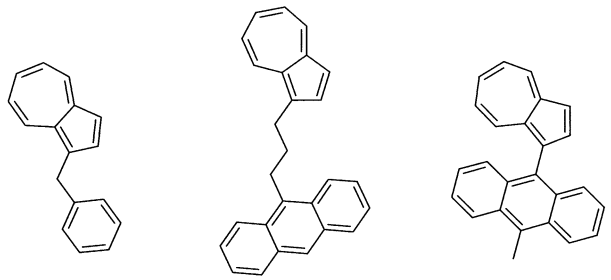

I **II** **III**

Figure 1. Molecular structures of 1-benzyl azulene (**I**), 9-(3-azulene-1-yl-propyl)-anthracene (**II**, Az-3-An), and 9-azulene-1-yl-10-methyl anthracene (**III**, Az-MeAn).

zeroth-order bright state. In particular for the liquid phase where the ability to resolve spectral features in detail is limited anyway, these methods combined with high time resolution have proven to be very powerful (see, e.g., refs 12−16 and references therein).

The present article is concerned with a more global IVR process, namely the transfer of vibrational energy through a chain of aliphatic carbon atoms. First attempts to determine how fast energy flows through carbon chains were made in the 1970s and 1980s preparing instable molecules or radicals which were chemically activated at a specific site. By analyzing dissociation products and comparing their rate of formation with a reference process, indirect information about the intramolecular energy flow was obtained.[17,18] In this context attention had been devoted to the question whether heavy atoms in the chain are able to block the intramolecular energy flux.[19−22] These experimental studies were accompanied by extensive numerical simulations.[23−26] Our present experiments provide a new, spectroscopic access to the phenomenon of intramolecular energy flow from one part into a distant other part of the molecule.

Our experimental approach to determine energy transfer rates through aliphatic chains relies on direct, time-resolved, experiments and employs the bridged azulene-aryl compounds **I**−**III** shown in Figure 1. The idea is to selectively excite the azulene side of these compounds by a short laser pulse and measure how fast the energy equilibrates within the whole molecule by transferring vibrational energy through the bridge to the remaining part of the molecule. This process can be followed directly by either probing the loss of vibrational energy at the azulene side (which was possible for compounds **I** and **II**), or the gain of energy at the anthracene side (compounds **II** and **III**). Additionally, due to the presence of additional extremely low-frequency vibrational modes in these compounds in comparison to azulene, their influence on the collisional vibrational energy transfer mechanism can be investigated by comparing CET rates of **I**−**III** with those of the bare azulene molecule.

II. Experimental Section

A. Experimental Approach. In our experiments the azulene side of compounds **I**−**III** was vibrationally excited with an excess energy of about 17240 cm^{-1} by $S_1 \leftarrow S_0$ absorption of a short laser pulse at 580 nm, followed by internal conversion back to the ground electronic state. For bare azulene, this preparation of highly vibrationally excited ground-state molecules is achieved within 1 ps or less.[27−29] In the case of the compounds **I**−**III**, the internal conversion rates k_{ic} were not known. Therefore, we determined k_{ic} in separate experiments such as described below. We found that again the excitation sequence is finished in less than 1 ps.

The loss of vibrational excitation at the azulene side of the molecules was monitored on the red wing of the azulene $S_3 \leftarrow S_0$ absorption band by probe pulses at a wavelength of about 300 nm. This method relies on the fact that electronic absorption spectra broaden once the vibrational energy inside the molecule is increased. Since the absorption is determined only by a few Franck−Condon-active modes, canonical and microcanonical spectra are essentially identical provided the internal energy in the molecule is the same.[30,31] Therefore, thermal "hot" spectra can be used to calibrate the energy content of molecules which are far from thermal equilibrium.

Similarly, for compounds **II** and **III**, the gain of vibrational energy at the anthracene side of the molecules, by IVR through the bridge, is monitored on the red wing of the anthracene $S_1 \leftarrow S_0$ absorption band using probe pulses of about 400 nm. For both chromophores, azulene and anthracene, the method of hot band absorption spectroscopy to monitor internal energies is well established.[4,5,32−36] For azulene, the energy dependence of absorption coefficients ϵ at 300 nm is characterized particularly well (see below), allowing for a conversion of transient absorption signals into energy loss curves. Since hot anthracene spectra were not available for calibration, we determined them in separate experiments, see below.

When the experiment is performed with isolated molecules the redistribution of vibrational energy proceeds until a microcanonical distribution is established. In solution, however, energy is removed by intermolecular vibrational energy transfer into the solvent until thermal equilibrium is achieved. To separate intra- and intermolecular energy transfer it is useful to choose a solvent for which vibrational energy transfer is particularly slow. We found that 1,1,2-trichloro-trifluoro-ethane ($C_2Cl_3F_3$) was an adequate solvent for our experimental objectives.

B. Experimental Technique. The required pump and probe pulses were obtained from a home-built Ti:sapphire oscillator-regenerative amplifier system which produced 80 fs laser pulses with energies of about 0.6 mJ near 800 nm and with a repetition rate of 1 kHz. Half of the energy was frequency doubled to 400 nm (60 μJ of pulse energy) and used to operate a one-stage nonlinearly pumped optical parametric amplifier (NOPA),[37] generating pulses in the range 550−620 nm which were needed for $S_1 \leftarrow S_0$ excitation of the azulene chromophore. Typical energies of these excitation pulses were in the range 6−10 μJ. After compression in a prism pair, part of this energy was frequency doubled in a 0.3 mm type-I KDP crystal in order to generate probe pulses in the range 290−310 nm of the $S_3 \leftarrow S_0$ absorption band of the azulene chromophore. To probe the anthracene chromophore, laser pulses around 400 nm had to be generated. These probe pulses were obtained by frequency doubling the remaining half of the 800 nm light in a 0.2 mm type-I BBO crystal.

The laser pulses were fed into a standard pump-and-probe interferometer, such as that described in Figure 1 of ref 38, attenuated, recombined, and collinearly focused into the sample cell. The relative plane of polarization was adjusted to 54.7° (magic angle) to remove all rotational contributions from the signal.[39] Probe energies were measured in front of and behind the sample by means of photodiodes. Behind the sample an interference filter for the probe wavelength was used to block transmitted excitation light. A synchronized chopper blocked every second pump pulse in order to independently measure eventual drifts of the background absorption. The time resolution, i.e., the width of the cross correlation between pump and probe pulses, in most cases was between 150 and 200 fs.

To determine S_1-lifetimes of the azulene chromophore, in compounds **I** and **III** we applied the two-photon fluorescence technique which was used previously to determine the S_1-lifetime of bare azulene and perdeutero azulene.[27,29,40−43] A first laser pulse excited the azulene-chromophore into the S_1-state which is depleted by internal conversion. A second, delayed, pulse was used to excite the surviving molecules in the S_1-state to the S_2-state from where they return to the ground state by emitting fluorescence. By recording the relative fluorescence yield as a function of the delay between both laser pulses, the internal conversion rate from the S_1-state was measured. For simplicity, we used pump and probe pulses of the same wavelength, splitting the output of the NOPA into two pulse trains of approximately equal energy that reached the sample with adjustable delay. Fluorescence was imaged onto the entrance slit of a monochromator and detected by a photomultiplier tube. All time-resolved experiments were performed in a quartz flow cell of 2 mm path length with polished side windows; samples consisting of about 10^{-3} M solutions of the respective compound in $C_2Cl_3F_3$ (Aldrich, purity > 99.9%) were employed.

For calibration of the "hot" absorptions, high-temperature thermal spectra of anthracene in the gas phase were determined in a quartz cell with an optical path length of 5 cm. The cell was filled with a known amount of anthracene dissolved in *n*-pentane, cooled to 250 K, evacuated to remove solvent and air, and then sealed off by melting. In this way the concentration of anthracene in the cell remained constant while heating in the spectrometer. Spectra were recorded in a temperature range of 420−700 K. They were supplemented by room-temperature spectra in *n*-hexane by accounting for the solvatochromic shift. The absorption spectra of anthracene and of the compounds **I**−**III** were recorded in a Cary 5E (Varian) spectrometer.

Azulene (purity > 98%) was purchased from Merck and used without further purification. All bridged azulene derivatives were synthesized in our laboratory. 1-benzyl azulene (**I**) was prepared by Friedel−Crafts alkylation of azulene with benzyl chloride following ref 44. Similarly, Az-MeAn (**III**) was obtained by reaction of azulene with 9-chloromethyl anthracene. For the preparation of Az-3-An (**II**), at first, 3-anthracene-9-yl-1-azulene-1-yl-propenone (Az-CO−CH═CH-An) was synthesized by Aldol condensation of 1-acetyl azulene and anthracene-9-carbaldehyde. Hydration of the central double bound by a mixture of formic acid and triethylamine, and reduction of the carbonyl group by lithium aluminum hydrate lead to the desired product. The compounds (**I**−**III**) were purified by column chromatography and recrystallization. The final purity proven by ^{1}H and ^{13}C NMR spectroscopy as well as by mass spectrometry was found to be better than 98%.

III. Results

A. Absorption Spectra. Room-temperature absorption spectra of the investigated compounds dissolved in $C_2Cl_3F_3$ are shown in Figure 2. Over the given wavelength range, the spectrum of 1-benzyl azulene (Figure 2a) is dominated by the azulene chromophore; apart from a red shift of about 800 cm^{-1} and small changes in the vibronic structure the spectra of **I** and azulene are nearly identical. Compared to gas-phase azulene, the 1-benzyl azulene spectrum is red-shifted at the long wavelength edge of the S_3-band by about 2200 cm^{-1}. As demonstrate below, this shift was taken into account when hot gas-phase spectra were used for calibration of time-resolved signals.

The reason anthracene was used as chromophore for measuring vibrational energy flow along aliphatic chains, is elucidated

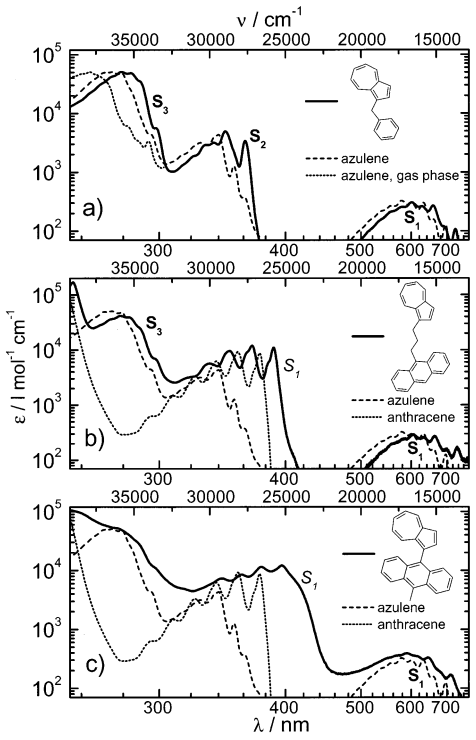

Figure 2. Absorption spectra of 1-benzyl azulene (a), Az-3-An (b), and Az-MeAn (c) in $C_2Cl_3F_3$ (spectra of azulene and anthracene in $C_2Cl_3F_3$, as well as azulene in the gas phase are shown for comparison; azulene and anthracene transitions, which are of relevance for the present experiments, are indicated by bold and italic letters, respectively).

in Figure 2b. The anthracene S_1-absorption band reaches about 20 nm into the gap between the S_1- and S_2-bands of azulene. At the same time, the azulene S_3-transition fills the gap between the S_1 and S_2-bands of anthracene. When both chromophores are combined in a single molecule, these transitions are still independent and can be used to monitor either the energy loss of azulene in its S_3-band or the energy gain of anthracene in its S_1-band. In fact, apart from small spectral shifts, the spectrum of Az-3-An can be considered as the sum of the individual azulene and anthracene spectra with well separated bands (one should note the logarithmic plots of ϵ in Figure 2).

For Az-MeAn, in principle one has to consider electronic interactions between the azulene and the anthracene chromophores because both π-electron systems are not sufficiently decoupled. When comparing Figs. 2b and 2c, a certain coupling indeed manifests itself by smearing out the features in the Az-MeAn absorption spectrum as compared to Az-3-An. However, the S_1-bands are still clearly separable, indicating that the ring systems are tilted. Since the azulene S_3-transition in Az-MeAn is not clearly separated, we investigated the IVR process only by probing the anthracene side at 400 nm.

Figures 3a and 4a show the absorption spectra of gaseous azulene and anthracene at various temperatures. In the case of azulene, the spectra were taken from previous static cell studies[36] and supplemented by shock wave experiments.[45] Since the vapor pressure of anthracene is too low at room temperature, the 303 K gas-phase spectrum in Figure 4a was constructed from a solution spectrum in *n*-hexane by shifting the latter to the blue by 880 cm^{-1} (The latter solvent shift was determined by comparing the 428 K gas-phase spectrum with an anthracene/*n*-hexane spectrum measured in a high-pressure cell at 428 K and a density corresponding to *n*-hexane at 1 bar and 303 K).

The absorption coefficients obtained from these static experiments were used to calibrate transient absorption signals in our

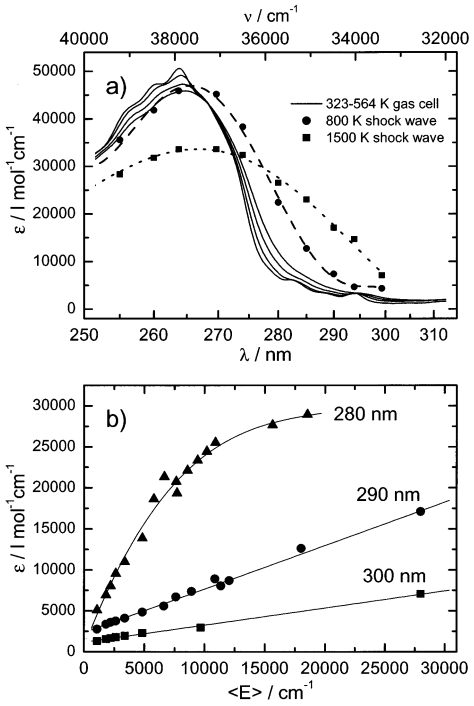

Figure 3. (a) Gas-phase absorption spectra of azulene at various temperatures. (b) Energy dependence of azulene absorption coefficient at selected wavelengths (from refs 36 and 45).

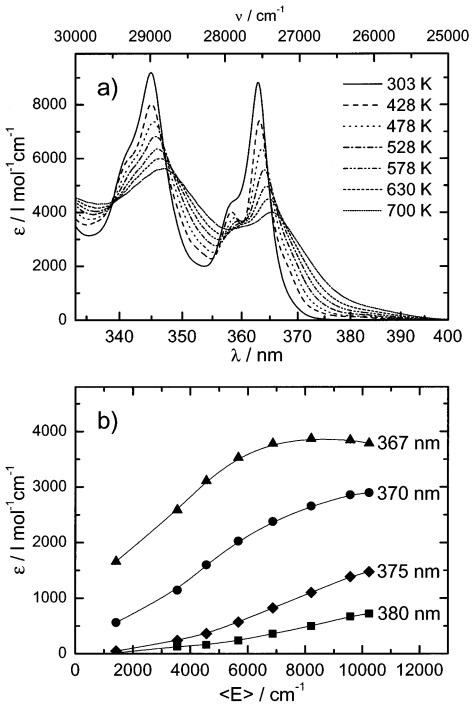

Figure 4. As Figure 3, for anthracene.

measurements. For this purpose, in Figures 3b and 4b, absorption coefficients at fixed wavelengts are plotted against the average vibrational energy $\langle E \rangle$ of the respective compounds. Average energies corresponding to the calibration temperatures were calculated from the normal-mode frequencies of azulene[46] and anthracene,[47] respectively.

B. S_1-lifetimes of the Azulene Chromophore. Figure 5 shows two-photon fluorescence signals of 1-benzyl azulene (Figure 5a) and Az-MeAn (Figure 5b) measured in $C_2Cl_3F_3$. Background fluorescence resulting from contributions of the

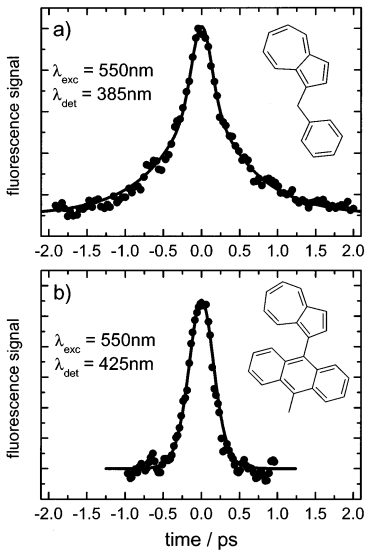

Figure 5. Two-photon fluorescence signal versus time delay between pump and probe pulse in $C_2Cl_3F_3$. Plotted are experimental data points and fits for (a) 1-benzyl azulene and (b) Az-MeAn. The evaluated S_1-lifetimes are 0.6 and <0.1 ps, respectively.

individual laser beams were of comparable magnitude as the signals of interest and were subtracted. Since pump and probe pulses had the same wavelength of 550 nm, both signals are symmetrical. For 1-benzyl azulene, the fluorescence was detected at 385 ± 10 nm which corresponds to the S_2-fluorescence of the azulene chromophore in this compound. In Az-MeAn, the anthracene S_1-state is energetically below the azulene S_2-state (see Figure 2). Therefore, one has also to consider electronic energy transfer leading to anthracene S_1 fluorescence at >420 nm which actually is displayed in Figure 5b.

The time dependent two-photon fluorescence signal of 1-benzyl azulene in Figure 5a consists of a faster and a slower exponentially decaying contribution. The latter can clearly be attributed to the S_1-lifetime of the azulene chromophore. The initial fast decay of the signal may arise from a nonresonant two-photon absorption into higher lying electronic states of azulene. In that case its width is determined by our time resolution, i.e., by the autocorrelation of the excitation pulses. Accordingly, the fit in Figure 5a is the sum of a Gaussian (representing the autocorrelation function of the laser pulses) and a symmetrized first-order decay function, $\exp(-|t|/\tau_{ic})$, convoluted with a Gaussian. The best agreement with the signal is obtained with an S_1 internal conversion time of $\tau_{ic} = 0.6$ ps and a fwhm of the Gaussian of 150 fs which is in accord with our actual time resolution. The S_1-lifetime of 1-benzyl azulene of 0.6 ps is shorter than the value measured previously for azulene. At comparable excess energies, Wurzer et al.[29] found biexponential decays of the two-photon fluorescence with time constants of $\tau_1 = 0.2$ ps and $\tau_2 = 0.8$ ps. While the slow component corresponds to internal conversion, the fast component was attributed to IVR of the initially excited bright states in the S_1 to dark background states. We cannot exclude that such a process also contributes to the fast initial decay in Figure 5a. However, it seems that for 1-benzyl azulene it must be considerably faster than the 200 fs found for azulene.[29] As shown in Figure 5b, the two-photon fluorescence signal of Az-MeAn decays extremely fast. Our analysis reveals that the S_1-lifetime approaches our time resolution such that we can only give an upper limit of $\tau_{ic} < 100$ fs for internal conversion of the azulene chromophore in Az-MeAn. In similar experiments

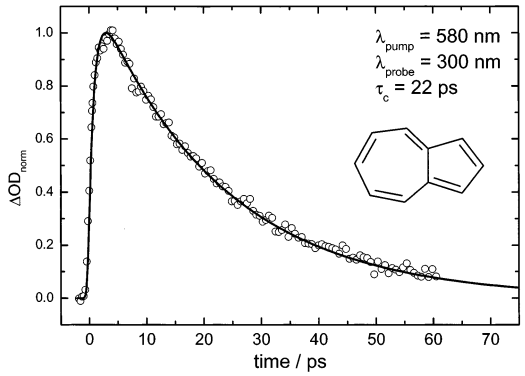

Figure 6. Absorption−time profile recorded during the vibrational energy transfer of azulene in $C_2Cl_3F_3$. The full line represents a fit assuming an exponential energy decay.

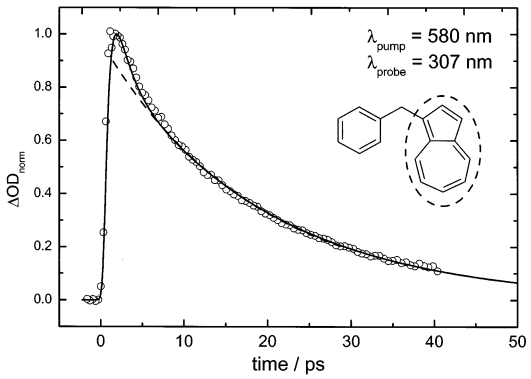

Figure 7. Absorption−time profile for 1-benzyl azulene in $C_2Cl_3F_3$ probing the energy content in the azulene chromophore (Cashed line: exponential energy decay at long times. Full line: energy diffusion model (see text)).

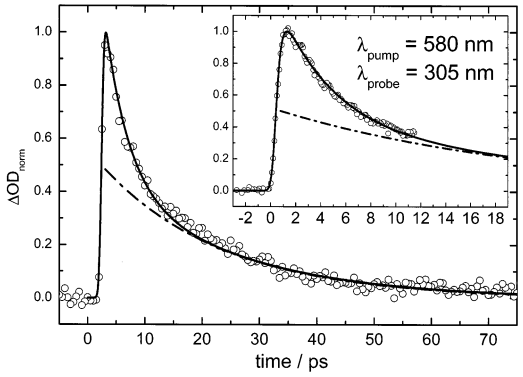

Figure 8. Absorption−time profile for Az-3-An in $C_2Cl_3F_3$ probing the vibrational energy in the azulene chromophore. (Dashed line: extrapolating exponential long-time decay to early times. Full line: energy diffusion model (see text); the insert enlarges the short time dynamics.)

on Az-3-An, the time constant for internal conversion in the S_1-state of the azulene chromophore was found to be $\tau_{ic} = 0.6$ ps.

C. Rates of Intra- and Intermolecular Energy Transfer. Before we present results for the bridged compounds **I**−**III**, a signal illustrating the loss of vibrational energy of excited bare azulene in $C_2Cl_3F_3$ is displayed in Figure 6, serving as a reference for our later analysis. After S_1-excitation at 580 nm, the absorption monitored at 300 nm at first increases with a time constant of about 1 ps, corresponding to the internal conversion of azulene. The increase of absorption is consistent with Figure 3; it demonstrates broadening of the $S_3 \leftarrow S_0$ band with enhanced absorption in the range 280−300 nm when the photon energy of 17240 cm^{-1} is transformed into vibrational excess energy in the ground electronic state. The subsequent decay of the signal in Figure 6 can be attributed to intermolecular energy transfer into the solvent. For a detailed analysis of this rate, in the following we assume that, apart from a solvatochromic shift $\Delta\lambda$, the hot azulene spectra in solution are the same as in the gas phase and that $\Delta\lambda$ is nearly temperature independent and can be determined from the room-temperature spectra. In this way the gas-phase calibration curves of Figures 3b (for azulene) and 4b (for anthracene) can be used to transform absorption signals into energy loss profiles. For azulene in $C_2Cl_3F_3$, e.g., $\Delta\lambda$ amounts to 10 nm (see Figure 2a). Since in the experiment of Figure 6 the probe wavelength was 300 nm, a gas-phase calibration curve $\epsilon_\lambda(\langle E\rangle)$ at $\lambda = (300-10)$ nm = 290 nm has to be used. In Figure 3b $\epsilon_{290}(\langle E\rangle)$ linearly depends on $\langle E\rangle$ such that the absorption signal in Figure 6 directly displays the energy loss of azulene in $C_2Cl_3F_3$. The assumption that hot spectra are besides a solvatochromic shift nearly identical in gas and liquid phase cannot be proven experimentally because during the energy transfer process in solution the surrounding liquid is essentially cold as was demonstrated by molecular dynamics simulations.[48] Therefore, even a steady state absorption spectrum measured in solution at high temperatures would not reflect the real experimental conditions. However, our previous results on the density dependence of azulene vibrational energy transfer are internally consistent indicating that possible errors caused by our analysis are negligible.[4,5,36]

In these earlier studies on azulene, we found that the energy loss under all experimental conditions is exponential and of the form $\langle E(t)\rangle = \langle E_0\rangle \exp(-t/\tau_c)$ where $\langle E_0\rangle$ is the photon energy of the excitation pulse and τ_c is a phenomenological cooling time constant. Applying this expression to Figure 6 and convoluting with the internal conversion process ($\tau_{ic} = 1$ ps) and the cross correlation of pump and probe pulses (Gaussian of 0.15 ps fwhm), perfect agreement with the recorded profile is obtained. A time constant of $\tau_c = 22$ ps corresponds to the solid line in the figure. The derived value of τ_c is estimated to be accurate within 10%.

We now present results for the bridged compounds **I**−**III**. The azulene S_3 absorption band in 1-benzyl azulene in solution is red-shifted by 17 nm with respect to the gas-phase azulene spectrum (Figure 2a). Therefore, when probing the energy transfer dynamics in 1-benzyl azulene at 307 nm (see Figure 7), one gets a direct image of the energy content in the azulene chromophore such as recorded at 290 nm, where the dependence of the absorption coefficient on energy $\epsilon(\langle E\rangle)$ is linear. In contrast to bare azulene, however, the energy loss in Figure 7 cannot be fitted by a single exponential. This is indicated by the dashed line matching the data points at times >5 ps and yielding a time constant of ∼20 ps. At shorter times there is clearly a faster drop of the internal energy with a time constant of about only 1.5 ps. The appearance of two separate time scales is even more pronounced for the compound Az-3-An such as demonstrated in Figure 8. To be in the linear $\epsilon(\langle E\rangle)$-regime, here we used a wavelength of 305 nm for probing the azulene chromophore, since the red-shift of its S_3-band amounts to 15 nm with respect to the gas phase (see Figure 2b). The signal consists of a fast decaying component (enlarged in the insert of Figure 8) with a time constant of about 4 ps and a slow one of about 20 ps.

A first interpretation of the two separate time scales in Figures 7 and 8 could be the assumption of a faster energy loss of the azulene chromophores by IVR toward intramolecular equilibrium and a subsequent slower intermolecular energy loss from

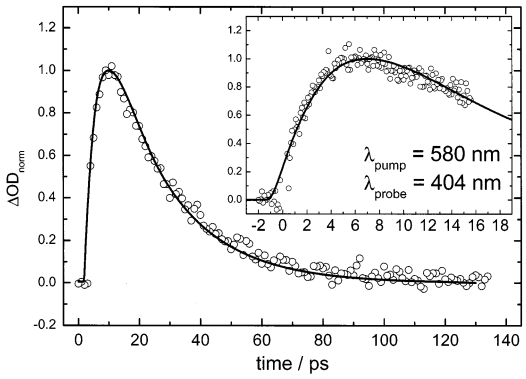

Figure 9. Absorption−time profile for Az-3-An in $C_2Cl_3F_3$ probing the vibrational energy in the anthracene chromophore (full line: energy diffusion model (see text); the insert enlarges the short time dynamics).

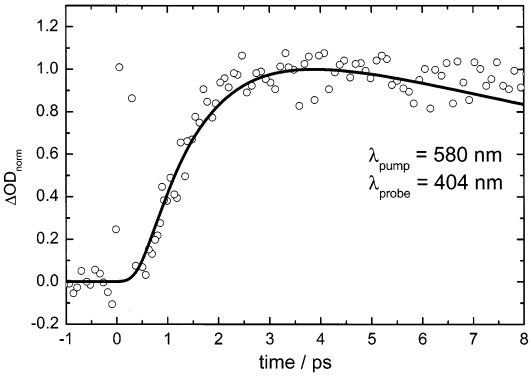

Figure 10. Absorption−time profile for Az-MeAn in $C_2Cl_3F_3$ probing the vibrational energy in the anthracene chromophore (full line: energy diffusion model (see text)).

the equilibrated molecules into the solvent. This view is supported by the fact that the time constants of the slower process are of similar magnitude as found for bare azulene. For this interpretation to be true, the two time scales also must be observed when the vibrational energy in the chromophore linked to azulene is probed. Figure 9 shows that indeed this is the case for the anthracene chromophore in Az-3-An. When probing the red edge of the anthracene S_1-band at 404 nm, after having excited the azulene side of the molecule, a rise of the signal within a few ps is observed which is followed by a much slower decay similar to Figures 6−8. Since the anthracene S_1-transition in Az-3-An is red-shifted by 26 nm with respect to isolated anthracene (cf. 2b and 4a), a probe wavelength of 404 nm for Az-3-An corresponds to the calibration curve of 378 nm for bare anthracene such as shown in Figure 4b. $\epsilon_{378}(\langle E \rangle)$, however, is nonlinear such that the signal in Figure 9 is not simply proportional to energy. This nonlinearity will be analyzed in more detail in section III.D. Despite this complication, the faster and slower time scales of about 3−4 and 20 ps from Figure 9 appear fully consistent with Figure 8 where the energy content of the azulene part of the molecule was monitored.

In Figure 10, an absorption−time profile of Az-MeAn in $C_2Cl_3F_3$ is shown, probing the internal energy in the anthracene chromophore after excitation of the azulene side of the molecule. Neglecting again the nonlinearity of the $\epsilon(\langle E \rangle)$ dependence at this stage, we observe a rise time of about 0.8 ps. In the previous section we have measured the internal conversion time of the azulene chromophore in Az-MeAn to be less than 100 fs. Therefore, we again attribute the observed rise in the absorption signal to the intramolecular energy flow from the azulene to the anthracene side of the molecule.

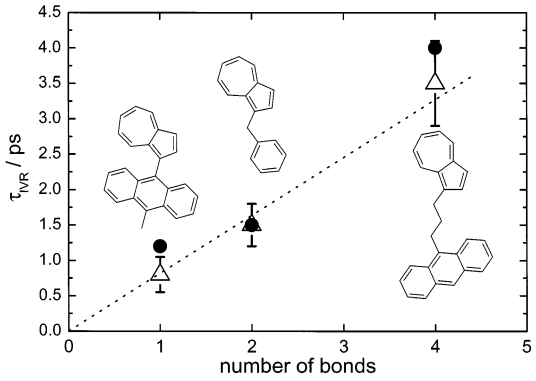

Figure 11. IVR times versus length of the aliphatic chain (open triangles: from exponential fits to the experimental curves; dotted line: linear fit to open triangles; full circles: from a global fit of eqs 2 and 3 to the data with constant $\kappa_{CC} = 10$ cm^{-1} K^{-1} ps^{-1}, see text).

D. Detailed Analysis of Intra- and Intermolecular Energy Transfer. The experimental IVR times τ_{IVR} reported in section III.C for the compounds **I**−**III** in Figure 11 are plotted vs the number of C−C bonds of the aliphatic chains connecting the two chromophores. To a good approximation there is a linear dependence between the number of C−C bonds and the time needed to reach microcanonical equilibrium inside the molecule. To rationalize this observation we design an energy diffusion model for intramolecular energy flow. We assume that intramolecular vibrational redistribution in both chromophores is faster than the energy flow through the bridge such that each chromophore acts as a thermal heat bath. If the heat capacity of the bridge is neglected, energy loss or gain may be described by an expression

$$\frac{dE}{dt} = -\kappa \frac{\Delta T(t)}{\Delta x} \tag{1}$$

where κ is the molecular energy conductivity of the carbon chain of length Δx and ΔT is the temperature difference between the chromophores. The distance can be expressed by the product $\Delta x = nl$, with the length l of an individual C−C-bond and the number n of bonds in the chain. Defining the molecular energy conductivity of a single C−C-bond by $\kappa_{CC} = \kappa/l$ and including an additional energy loss term describing the intermolecular vibrational energy transfer into the solvent, one has

$$\begin{pmatrix} \frac{dE_1(t)}{dt} \\ \frac{dE_2(t)}{dt} \end{pmatrix} = \begin{pmatrix} \frac{\kappa_{CC}}{n}[T_2(t) - T_1(t)] - \frac{E_1(t) - E_{th,1}}{\tau_{c,1}} \\ \frac{\kappa_{CC}}{n}[T_1(t) - T_2(t)] - \frac{E_2(t) - E_{th,2}}{\tau_{c,2}} \end{pmatrix} \tag{2}$$

where $\tau_{c,1}$ and $\tau_{c,2}$ are the characteristic times for collisional energy loss into the solvent, and $E_{th,1}$ and $E_{th,2}$ are thermal energies at 300 K of the chromophores, respectively. Equation 2 corresponds to exponential energy loss of the whole molecule through intermolecular energy transfer, in agreement with our previous studies on bare azulene.[36]

The energies E_1 and E_2 at a given temperature T are calculated from the s normal-mode frequencies ν_i of the respective chromophore via

$$E(T) = \sum_{i=1}^{s} \frac{h\nu_i}{\exp(h\nu_i/k_BT) - 1} \tag{3}$$

The frequencies of azulene,[46] benzene,[49] and anthracene[47] were

taken from the literature. Equation 3 defines the vibrational temperature T for a given internal energy. (One should note that, throughout this article, energies for convenience were represented in cm^{-1}).

Equations 2 and 3 are solved, starting from the initial condition that the azulene vibrational energy at $t_0 = 0$ is the sum of its thermal energy and the photon energy $E_{exc} = 17240$ cm^{-1} of the pump pulse $E_1(t_0) = E_{th,1} + E_{exc}$, whereas the energy of the other chromophore is $E_2(t_0) = E_{th,2}$. Once the energy is equilibrated between the two chromophores by IVR, the subsequent collisional energy loss of the whole molecule in principle is characterized by some average τ_c of $\tau_{c,1}$ and $\tau_{c,2}$. Since the experiment is only sensitive to this average, we replace $\tau_{c,1}$ and $\tau_{c,2}$ by τ_c. In this way, only two adjustable parameters, namely τ_c and κ_{CC}, remain to be fitted from the experimental profiles shown in Figures 7−10. In doing this, we tentatively assumed that the molecular energy conductivity per single C−C-bond is constant for all investigated molecules.

The time dependent energies $E_1(t)$ and $E_2(t)$ in eqs 2 and 3 were transformed into absorption changes $\Delta\epsilon(t)$ by means of the calibration curves for $\epsilon_\lambda(\langle E\rangle)$ given in Figures 3 and 4, taking into account the probe wavelengths λ and the relevant solvatochromic shifts. Finally, $\Delta\epsilon(t)$ was convoluted with the internal conversion process preceding IVR (exponential with time constant τ_{ic}) and the finite time resolution of the experiment (Gaussian with 0.15 ps fwhm). The results of this analysis are the full lines in Figures 7−10. With an energy conductivity per C−C-bond of $\kappa_{CC} = (10 \pm 1)$ cm^{-1} K^{-1} ps^{-1} (=120 J mol^{-1} K^{-1} ps^{-1}), and a time constant of $\tau_c = (21 \pm 2)$ ps for intermolecular energy transfer, remarkable agreement with the experimental data is obtained. The amplitude ratios of the fast and slow energy loss, obtained by probing the azulene side in 1-benzyl azulene (Figure 7) and Az-3-An (Figure 8) are reproduced particularly well. The time evolutions of the vibrational energies and temperatures, corresponding to our evaluation of the experiments, are shown in Figures 12 and 13. In 1-benzyl azulene, the IVR process equilibrating the vibrational energy between azulene and benzene is complete within about 6 ps (see lower part of Figure 12). During this time the benzene part of the molecule reaches a maximum energy of 5000 cm^{-1} (corresponding to a maximum temperature of about 800 K). After this period, the excess energy in the molecule is transferred to the solvent within several tens of picoseconds. During this later stage of the process, the energy of benzene due to its smaller heat capacity is always below that of azulene. After convolution of the azulene $E(t)$ curve with the preceding internal conversion process of 0.6 ps only a small portion of the fast decaying component remains as shown in Figure 7. In contrast, for Az-3-An the equilibration between azulene and anthracene takes considerably longer than in 1-benzyl azulene (about 20 ps, see lower part of Figure 13). Also, the amplitude of the fast energy loss of the azulene chromophore leading to microcanonical equilibrium is increased. The reason is the larger distance between the two chromophores as well as the larger heat capacity of anthracene in comparison to benzene. The dependence of τ_{IVR} on the heat capacities c_1 and c_2 of azulene and the energy acceptor can easily be rationalized when for a while we assume c_1 and c_2 to be constant such that $E = cT$. Then eq 1 can be solved analytically and the energy loss (gain) of azulene (the acceptor) toward microcanonical equilibrium is found to be exponential with a time constant of $\tau_{IVR} = (1/c_1 + 1/c_2)^{-1}\, n/\kappa_{CC}$, i.e., the larger c_1 and c_2 the longer the IVR-times. Therefore, the deviations from linearity shown in Figure 11 can entirely be attributed to variations of the heat capacity as the energy acceptor changes.

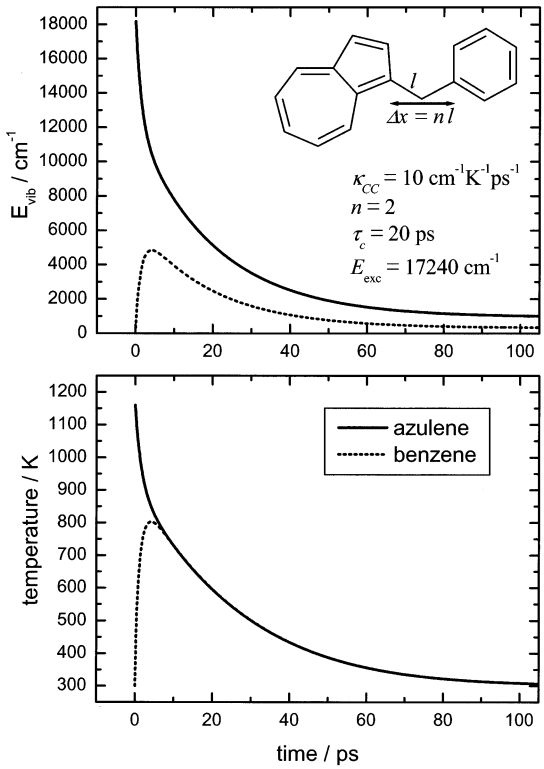

Figure 12. Time evolution of the vibrational energy and temperature in the azulene and benzene part of 1-benzyl azulene according to the diffusion model of eqs 2 and 3.

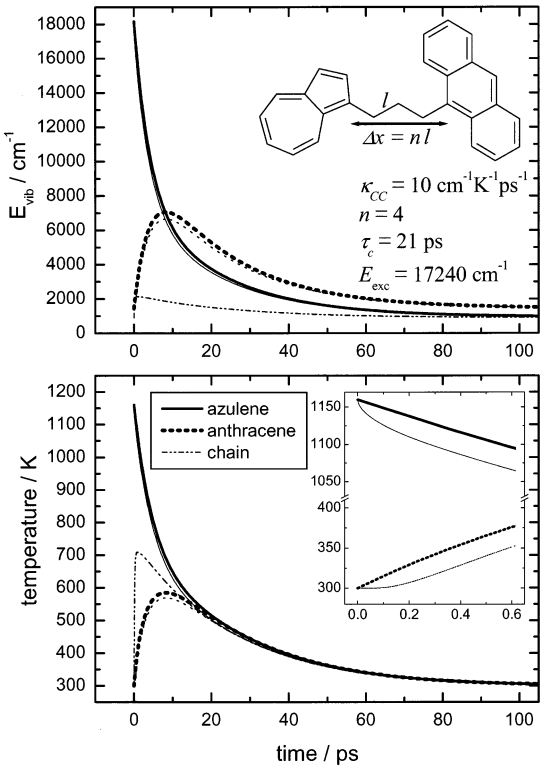

Figure 13. Time evolution of the vibrational energy and average temperature in different parts of the Az-3-An molecule. (Thick lines: neglecting the heat capacity of the chain, eqs 2 and 3. Thin lines: with constant heat capacity of the chain of $c_3 = 3$ cm^{-1}/K, see text).

The simulated energy-time profiles in Figures 12 and 13 (and also for Az-MeAn, not shown here) can be fitted by simple

functions. For azulene, a biexponential decay of the form

$$E(t) = E_{IVR} \exp(-t/\tau_{IVR}) + E_c \exp(-t/\tau_c) + E_{th} \quad (4)$$

applies where E_{IVR} and E_c are the amplitudes associated with the intra- and intermolecular energy transfer processes. The energy of benzene (anthracene) can be expressed by

$$E(t) = E_0\left(\frac{1/\tau_{IVR}}{1/\tau_{IVR} - 1/\tau_c}\right)[\exp(-t/\tau_c) - \exp(-t/\tau_{IVR})] + E_{th} \quad (5)$$

The derived fit parameters and corresponding errors are summarized in Table 1. τ_{IVR} derived from the detailed analysis are shown in Figure 11 by full circles. They are consistent with the IVR times obtained by simply fitting of the experimental traces by sums of exponentials (open triangles). The difference for Az-MeAn results from the fact that in the first analysis the nonlinearity of the calibration curve $\epsilon_\lambda(\langle E\rangle)$ was not taken into account.

In a more refined energy diffusion model one has to consider the heat capacity c_3 of the aliphatic chain. Then the energy flux through the chain may be described by

$$\frac{\partial T}{\partial t} = \beta\frac{\partial^2 T}{\partial x^2} \quad (6)$$

where $\beta = \kappa/c_3$ is the thermal diffusivity of the chain. At both ends of the chain energy conservation is obtained involving the flux analogous to eq 1. This approach was tested for Az-3-An, the compound with the longest chain because there the strongest deviations from the simpler model with $c_3 = 0$ should appear. The heat capacity of the $(CH_2)_3$-chain was estimated from the normal-mode frequencies of propane to be $c_3 = 3$ cm^{-1}/K.[50] For simplicity we assumed this quantity to be independent of temperature. The results of corresponding calculations (see thin lines in Figure 13) differ only slightly from the approximate model with $c_3 = 0$. The insert in the lower part of Figure 13 demonstrates that the difference arises from the fact, that the energy needs about 200 fs to pass and heat up the chain and finally enter the anthracene side. Shortly after that, a constant (but time dependent) temperature gradient within the chain is established and the subsequent evolution of the intramolecular energy flow is adequately described by eq 1. Since the time resolution of the experiment is limited by the internal conversion process taking 0.6 ps for Az-3-An, the 200 fs transient cannot be resolved. Therefore, the error caused by neglecting the heat capacity of the chain is of minor importance.

IV. Discussion

Our experiments, first, provide new information on the question to what extent low-frequency modes of the highly excited molecules govern intermolecular energy transfer into liquid solvents. The results summarized in Table 1 indicate that for this energy transfer in liquid $C_2Cl_3F_3$, the characteristic time τ_c is practically identical for bare azulene, 1-benzyl azulene, Az-MeAn, and Az-3-An. To identify the role of low-frequency modes, we have performed DFT calculations for 1-benzyl azulene. While the lowest frequency of azulene is at 189 cm^{-1},[46] for 1-benzyl azulene we found six modes with lower frequencies, being in the range 9−178 cm^{-1}. Apparently, the presence of these additional low-frequency modes has no influence on the energy transfer in liquid $C_2Cl_3F_3$. The observation, that the addition of lower frequency modes has no influence on τ_c, seems to contradict a series of experimental[51−53] and theoretical[54] results for collisional energy transfer of highly excited polyatomics in a variety of bath gases. In this case, low-frequency modes often seemed to govern the efficiency of energy exchange. This is not the place to discuss the mechanism and quantitative details of intermolecular energy transfer of highly excited molecules. However, it should be emphasized that apparently there is a marked change in the mechanism of intermolecular energy transfer from low-pressure gas phase to dense fluid conditions. The numerical simulations in ref 7 (see Figures 3 and 4 from ref 7) showed that the lowest frequency modes governed the energy exchange in isolated binary collisions; in contrast to this, at high densities the dominant importance of the lowest frequency modes disappears and almost all modes contribute. As is apparent in Figure 1 from ref 7, during energy transfer at high densities the energy in low-frequency modes is below the expected value, if the internal energy were equilibrated over the whole molecule. This suggests that the reason for the change in the mechanism can be attributed to inefficient repopulation of low-frequency modes by incomplete IVR. Applying these results to our bridged azulene compounds we have to conclude that during intermolecular vibrational energy transfer the low-frequency vibrational modes in the bridged azulene-aryl derivatives (**I**−**III**) apart from their thermal energy are essentially not populated because τ_c is the same as for bare azulene. This interpretation is not necessarily in contradiction to our experimental studies on energy transfer of bare azulene from the gas into dense fluid phase, which indicated that τ_c changes with the local density such as expressed by the radial distribution function at contact between the colliders.[4,5] There an influence of the density on the average energy $\langle\Delta E\rangle$ transferred per binary collision apparently was not observed. It might, however, be that the applied collision model is flexible enough to cover changes of the energy transfer mechanism. Further theoretical studies have to shed light on this aspect of intermolecular energy transfer.

Our observations of intramolecular energy flow, from one chromophore through an aliphatic bridge to another chromophore, apparently concern an overall aspect of IVR while finer details were not resolved. We even have no information on whether our results correspond to a property of isolated molecules or whether IVR is collision-assisted under our conditions. It is well-known that IVR in isolated molecules often follows very specific pathways, with hierarchies of processes on different time scales.[10,11,1] Our observation of an energy diffusivity, which is proportional to the length of the aliphatic bridge, seems to indicate a fairly unspecific overall behavior of IVR. It appears desirable to collect more experimental information on the phenomenon, with different types of bridges

TABLE 1: Parameters of Equations 4 and 5 to Describe Energy-Time Profiles Derived from Model Calculations, Considering Energy Diffusion through the Aliphatic Chains with Constant $\kappa_{CC} = 10$ cm^{-1} K^{-1} ps^{-1}

	bare azulene	1-benzyl azulene	Az-3-An	Az-MeAn
eq 4	azulene	azulene	azulene	azulene
E_{th}/cm^{-1}	940	940	940	940
E_{IVR}/cm^{-1}	0	6080 ± 500	10200 ± 500	10050 ± 500
E_c/cm^{-1}	17240	11160 ± 500	7040 ± 500	7190 ± 500
τ_{IVR}/ps	−	1.5 ± 0.2	4.0 ± 0.4	1.2 ± 0.1
τ_c/ps	22 ± 2	20 ± 2	21 ± 2	21 ± 2
eq 5		benzene	anthracene	anthracene
E_{th}/cm^{-1}		310	1440	1440
E_0/cm^{-1}		5610 ± 500	8270 ± 500	9500 ± 500
τ_{IVR}/ps		1.5 ± 0.2	4.0 ± 0.4	1.2 ± 0.1
τ_c/ps		20 ± 2	21 ± 2	21 ± 2

and greater lengths. In addition, new theoretical simulations should be made.

It should be mentioned that related experiments with azulene-$(CH_2)_n$-coumarine 151 (with $n = 1$ or 3) in ref 55 were interpreted in terms of longer IVR times (5−30 ps) and shorter times for intermolecular energy loss (less than 7 ps); in addition, no dependence of IVR on n was realized. As the time resolution of the studies in ref 55 was only 5 ps, the interpretation of these results may not have been conclusive.

The present results for IVR through aliphatic chains are more closely linked to the chemical activation studies from.[17,18,56,57] In these experiments a large amount of energy enters a localized region of a substrate molecule by reaction with radicals at a specific site. The activated species subsequently are able to decompose via different reaction channels depending on whether the energy is randomized over the whole molecule or not. Alternatively, the species can be stabilized by collisions with a buffer gas. By analyzing product ratios as function of gas pressure, indirect information about the IVR process was obtained with the collision frequency serving as a clock for the IVR rate. In this way, for example, an energy randomisation time between both cyclopropyl-rings in vibrationally excited hexafluorobicyclopropyl-d_2 of 0.9 ps was found.[17] Since chemical activation experiments of this type yield IVR times under collision free conditions the consistency with our values seems to indicate that collisions do not markedly accelerate intramolecular energy flow.

Contrary to these studies on molecules with a carbon skeleton, Rogers and co-workers investigated the reaction of tetraallyl tin and tetraallyl germanium with fluorine atoms.[19,20] Here, the deduced rate constant for the decomposition of the formed radical was 1000 times larger than that predicted from RRKM theory suggesting that the central heavy atom, Sn or Ge, blocks the intramolecular flow of vibrational energy. The heavy atom effect was also found in spectroscopic IVR studies on the alkyne series of the type $(CH_3)_3XC{\equiv}C-H$, with X = C, Si, or Sn, after overtone excitation of the C−H-stretch vibration.[11] Computer simulations on related model systems, however, indicate that a change in the intramolecular potential rather than a change in the mass dominates the observed phenomenon.[23,25,58−60] Currently, we are preparing compounds of the type **I**−**III** with modified bridges to investigate the influence of heteroatoms in the chain on intramolecular energy flow.

V. Conclusions

In the present work we have investigated intramolecular vibrational energy flow through aliphatic chains and vibrational energy transfer into a liquid solvent, for bridged azulene-aryl compounds dissolved in $C_2Cl_3F_3$, using time-resolved spectroscopy. After S_1 laser excitation and subsequent internal conversion of the azulene chromophore the IVR/CET dynamics was monitored with a probe pulse at the azulene and/or the aryl site, employing the hot band absorption technique. The time scales of intramolecular energy flow and energy transfer to the bath are well separated. For chain lengths between 1 and 4 C−C bonds, the IVR times were found to vary between 1.2 and 4.0 ps, whereas the CET time constants of $\tau_c = (21 \pm 2)$ ps are nearly independent of the substituent and the same as for the bare azulene molecule. Combining an energy diffusion model for the IVR process with an exponential model for the energy decay of the whole molecule, excellent agreement with the experimental data is achieved. For the investigated compounds, our analysis yields a constant energy conductivity of the C−C-bond of $\kappa_{CC} = (10 \pm 1)$ cm^{-1} K^{-1} ps^{-1} (=120 J mol^{-1} K^{-1} ps^{-1}). The insensitivity of τ_c on the presence of additional, partially extremely low-frequency, vibrational modes in the bridged azulene-aryl compounds in comparison to azulene indicates that these modes do not participate in the IVR/CET process.

Acknowledgment. The authors are grateful to Dr. Wolfgang Kühnle, Jürgen Bienert, and Jens Schimpfhauser for the preparation and purification of the investigated azulene derivatives. We also thank Dr. Simone Techert for cooperation in performing DFT calculations.

References and Notes

(1) Nesbitt, D. J.; Field, R. W. *J. Phys. Chem.* **1996**, *100*, 12735.
(2) Gilbert, R. G.; Smith, S. C. *Theory of Unimolecular and Recombination Reactions*; Blackwell Scientific: Cambridge, MA, 1990.
(3) Baer, T.; Hase, W. L. *Unimolecular Reaction Dynamics*; Oxford: New York, 1996.
(4) Schwarzer, D.; Troe, J.; Zerezke, M. *J. Chem. Phys.* **1997**, *107*, 8380.
(5) Schwarzer, D.; Troe, J.; Zerezke, M. *J. Phys. Chem. A* **1998**, *102*, 4207.
(6) Chesnoy, J.; Gale, G. M. *Ann. Phys. Fr.* **1984**, *9*, 893.
(7) Heidelbach, C.; Schroeder, J.; Schwarzer, D.; Vikhrenko, V. S. *Chem. Phys. Lett.* **1998**, *291*, 333.
(8) Heidelbach, C.; Vikhrenko, V. S.; Schwarzer, D.; Schroeder, J. *J. Chem. Phys.* **1999**, *110*, 5286.
(9) Käb, G.; Schröder, C.; Schwarzer, D. *Phys. Chem. Chem. Phys.* **2002**, *4*, 271.
(10) Quack, M. *Annu. Rev. Phys. Chem.* **1990**, *41*, 839.
(11) Lehmann, K. K.; Scoles, G.; Pate, B. H. *Annu. Rev. Phys. Chem.* **1994**, *45*, 241.
(12) Laubereau, A.; Kaiser, W. *Rev. Mod. Phys.* **1978**, *50*, 607.
(13) Seifert, G.; Zürl, R.; Graener, H. *J. Phys. Chem. A* **1999**, *103*, 10749.
(14) Woutersen, S.; Emmerichs, U.; Bakker, H. J. *Science* **1997**, *278*, 658.
(15) Bingemann, D.; King, A. M.; Crim, F. F. *J. Chem. Phys.* **2000**, *113*, 5018.
(16) Charvat, A.; Assmann, J.; Abel, B.; Schwarzer, D. *J. Phys. Chem. A* **2001**, *105*, 5071.
(17) Rynbrandt, J. D.; Rabinovitch, B. S. *J. Phys. Chem.* **1971**, *75*, 2164.
(18) Wrighley, S. P.; Rabinovitch, B. S. *Chem. Phys. Lett* **1983**, *95*, 363.
(19) Rogers, P.; Montague, D. C.; Frank, J. P.; Tyler, S. C.; Rowland, F. S. *Chem. Phys. Lett* **1982**, *89*, 9.
(20) Rogers, P. J.; Selco, J. I.; Rowland, F. S. *Chem. Phys. Lett.* **1983**, *97*, 131.
(21) Wrighley, S. P.; Rabinovitch, B. S. *Chem. Phys. Lett.* **1983**, *98*, 386.
(22) Wrighley, S. P.; Oswald, D. A.; Rabinovitch, B. S. *Chem. Phys. Lett.* **1984**, *104*, 521.
(23) Lopez, V.; Marcus, R. A. *Chem. Phys. Lett.* **1982**, *93*, 232.
(24) Schranz, H. W.; Nordholm, S.; Freasier, B. C. *Chem. Phys.* **1986**, *108*, 69.
(25) Uzer, T.; Hynes, J. T. *Chem. Phys.* **1989**, *139*, 163.
(26) Sumpter, B. G.; Noid, D. W. *Chem. Phys.* **1992**, *160*, 393.
(27) Schwarzer, D.; Troe, J.; Schroeder, J. *Ber. Bunsen-Ges. Phys. Chem.* **1991**, *95*, 933.
(28) Ruth, A. A.; Kim, E.-K.; Hese, A. *Phys. Chem. Chem. Phys.* **1999**, *1*, 5121.
(29) Wurzer, A. J.; Wilhelm, T.; Piel, J.; Riedle, E. *Chem. Phys. Lett.* **1999**, *299*, 296.
(30) Hippler, H.; Troe, J.; Wendelken, H. J. *J. Chem. Phys.* **1983**, *78*, 6709.
(31) Quack, M. *Nuovo Cimento* **1981**, *B63*, 1981.
(32) Gottfried, N. H.; Seilmeier, A.; Kaiser, W. *Chem. Phys. Lett.* **1984**, *111*, 326.
(33) Wild, W.; Seilmeier, A.; Gottfried, N. H.; Kaiser, W. *Chem. Phys. Lett.* **1985**, *119*, 259.
(34) Sukowski, U.; Seilmeier, A.; Elsaesser, T.; Fischer, S. F. *J. Chem. Phys.* **1990**, *93*, 4094.
(35) Hippler, H.; Otto, B.; Troe, J. *Ber. Bunsen-Ges. Phys. Chem.* **1989**, *93*, 428.
(36) Schwarzer, D.; Troe, J.; Votsmeier, M.; Zerezke, M. *J. Chem. Phys.* **1996**, *105*, 3121.
(37) Wilhelm, T.; Piel, J.; Riedle, E. *Opt. Lett.* **1997**, *22*, 1494.
(38) Nikowa, L.; Schwarzer, D.; Troe, J.; Schroeder, J. *J. Chem. Phys.* **1992**, *97*, 4827.

(39) Fleming, G. R. *Chemical Applications of Ultrafast Spectroscopy*, 1st ed.; Oxford University Press: New York, 1986.
(40) Ippen, E. P.; Shank, C. V.; Woerner, R. L. *Chem. Phys. Lett.* **1977**, *46*, 20.
(41) Shank, C. V.; Ippen, E. P.; Teschke, O.; Fork, R. L. *Chem. Phys. Lett.* **1978**, *57*, 433.
(42) Nibbering, E. T. J.; Duppen, K.; Wiersma, D. A. Non-Markovian Dynamics of Azulene in Solution. In *Ultrafast Phenomena 'VII*; Springer-Verlag: Berlin, 1990; p 471.
(43) Wagner, B. D.; Szymanski, M.; Steer, R. P. *J. Chem. Phys.* **1993**, *98*, 301.
(44) Anderson, A. G.; Cowles, E. J.; Tazuma, J. J.; Nelson, J. A. *J. Am. Chem. Soc.* **1955**, *77*, 6321.
(45) Brouwer, L.; Hippler, H.; Lindemann, L.; Troe, J. *J. Phys. Chem.* **1985**, *89*, 4608.
(46) Chao, R. S.; Khanna, R. K. *Spectrochim. Acta* **1977**, *31A*, 53.
(47) Chakraborty, D.; Ambashta, R.; Manogaran, S. *J. Phys. Chem.* **1996**, *100*, 13963.
(48) Heidelbach, C.; Fedchenia, I. I.; Schwarzer, D.; Schroeder, J. *J. Chem. Phys.* **1998**, *108*, 10152.
(49) Handy, N. C.; Maslen, P. E.; Amos, R. D.; Andrews, J. S.; Murray, C. W.; Laming, G. J. *Chem. Phys. Lett.* **1992**, *197*, 506.
(50) Schachtschneider, J. H.; Snyder, R. G. *Spectrochim. Acta* **1963**, *19*, 117.
(51) Toselli, B. M.; Barker, J. R. *J. Chem. Phys.* **1992**, *97*, 1809.
(52) Brenner, J. D.; Erinjeri, J. P.; Barker, J. R. *Chem. Phys.* **1993**, *175*, 99.
(53) Damm, M.; Hippler, H.; Olschewski, H. A.; Troe, J.; Willner, J. *Z. Phys. Chem. N. F.* **1990**, *166*, 129.
(54) Lenzer, T.; Luther, K.; Troe, J.; Gilbert, R. G.; Lim, K. F. *J. Chem. Phys.* **1995**, *103*, 626.
(55) Okazaki, T.; Hirota, N.; Nagata, T.; Osuka, A.; Terazima, M. *J. Phys. Chem. A* **1999**, *103*, 9591.
(56) Oref, I.; Rabinovitch, B. S. *Acc. Chem. Res.* **1979**, *12*, 166.
(57) Trenwith, A. B.; Rabinovitch, B. S. *J. Chem. Phys.* **1986**, *85*, 1694.
(58) Swamy, K. N.; Hase, L. *J. Chem. Phys.* **1985**, *82*, 123.
(59) Schranz, H. W.; Nordholm, S.; Freasier, B. C. *Chem. Phys.* **1986**, *108*, 105.
(60) Stuchebrukhov, A. A.; Marcus, R. A. *J. Chem. Phys.* **1993**, *98*, 6044.